Crystallization behavior and IR structure of yttrium aluminosilicate glasses

ZHENG, Q., LIU, Y., LI, M., LIU, Z., HU, Y., ZHANG, X., DENG, Wei and WANG, M.

Crystallization behavior and IR structure of yttrium aluminosilicate glasses

Qingshuang Zheng[1, 2], Yucheng Liu[1, 2], Mei Li[1, 2, 3]*, Zhaogang Liu[2, 3], Yanhong Hu[2, 3], Xiaowei Zhang[1, 2, 3], Wei Deng[4], Mitang Wang[1, 2, 3]*

(1 School of Materials Science and Engineering, University of Shanghai for Science and Technology, Shanghai 200093, China;

2 School of Material and Metallurgy, Inner Mongolia University of Science and Technology, Baotou 014010, China;

3 Key Laboratory of Green Extraction & Efficient Utilization of Light Rare-Earth Resources, Ministry of Education, Baotou 014010, China;

4 Materials and Engineering Research Institute, Sheffield Hallam University, Sheffield S1 1WB, UK)

Abstract: The crystallization of four Y_2O_3-Al_2O_3-SiO_2 (YAS) glasses were investigated to prepare YAS glass ceramics precipitated singly/mainly $Y_2Si_2O_7$ or $Y_{4.67}(SiO_4)_3O$ apatite, and to explore the crystallization difference between the stoichiometric parent glass (SPG) and non-stoichiometric parent glass (NSPG). The DSC results revealed that glass locating at the higher liquidus surface temperature has lower crystallization peak temperature, which indicating that the corresponding glass has higher crystallization potential to crystallize easily. Crystallization of the NSPG samples is along surface and caused by phase separation, while SPG sample is the surface crystallization at the first

exothermic peak temperature and overall crystallization at the second exothermic peak temperature. Glass ceramics only containing y-$Y_2Si_2O_7$ or $Y_{4.67}(SiO_4)_3O$ apatite are obtained successfully, and which are illustrated by fitting FTIR spectra. These results can provide technical guide for controlling the crystallization process and the types of precipitated crystals in YAS glass for different application potentials.

Keywords: Crystallization; Y_2O_3; Glass ceramics; Structure

1. Introduction

Yttrium aluminosilicate (YAS) glass and glass ceramics have attracted much attention due to their numerous excellent properties [1-8]. The low thermal expansion coefficients (TECs) makes YAS glasses promising for application as adhesives for joining, especially for the non-oxide ceramics such as SiC and Si_3N_4 [3,4]. YAS system glass has interesting chemical durability [5,6], so the glass can prepare glass microspheres (including Yttrium-89) used to treat cancers [6,7]. YAS glasses and glass ceramics can accommodate high concentration of rare earth ions and have great potential for optical applications [8]. YAS glasses are also used in optical fibers and corresponding glass ceramics can be used as a matrix for storage of long-lived actinides [9-11].

Types of crystal precipitated have great influence on the properties of glass ceramics, thereby it is essential to explore clearly the crystallization of YAS glass. The YAS glass-forming zone includes $Y_2Si_2O_7$, SiO_2, mullite and Al_2O_3 phase region in the

Y_2O_3-Al_2O_3-SiO_2 phase diagram [9, 12]. Najim Sadiki et al. [9] studied four compositions of YAS glass melted by a laboratory-scale solar furnace, they found that mullite, SiO_2, y-$Y_2Si_2O_7$ and a little β-$Y_2Si_2O_7$ can be crystallized in studied glass, but two or three crystals were precipitated finally from each glass for these compositions. S. Ahmadet al. [13] found unknown phase for YAS glass ceramic during high temperature long heat treatments, and the chemical composition of the unknown phase is determined to be Y = 8.45, Si = 16.45, Al = 12.82 and O = 62.26 (at. %). Yttrium silicates, including $Y_2Si_2O_7$, Y_2SiO_5 and $Y_{4.67}(SiO_4)_3O$ apatite, have many potential applications such as high-temperature structural ceramics, oxidation protective coatings and environmental barrier coatings, because of their specific mechanical, thermal, tribological and dielectric properties and environmental durability [14]. YAS glass ceramics are superior than YAS glasses in mechanical performance and oxidation resistance when they are used as sintering additives for preparing SiC ceramic or Si_3N_4 ceramic [15]. Matching TECs of the joined components and filler is essential for minimizing the thermal stresses in the joint, so that the thermal expansion coefficients of sintering additives or filler should be in the same range or lower than those of the ceramic materials to be joined [3]. As the sintering additives or filler, the TEC of YAS glass ceramics depends on the all components including precipitated crystal types and contents, as well as residual glass content and compositions. It is well known that the thermal expansion coefficient of $Y_2Si_2O_7$ is smaller than other kind of crystals precipitated in YAS glass

ceramics and hence $Y_2Si_2O_7$ phase would be in the best interest for YAS glass filler with lower TEC. Besides, apatite-type rare earth silicates have been found to have the low activation energy in the ionic conduction, and thus it is suitable for an intermediate-temperature solid oxide fuel cells (SOFC) electrolyte [16]. Recently, Liao T et al. [17] investigated the position preference and diffusion mechanisms of interstitial oxygen ions in lanthanum silicate $La_{9.33}Si_6O_{26}$ using density functional theory. For the yttrium silicate ($Y_{4.67}(SiO_4)_3O$ apatite), it can be prepared by hydrothermal method, solid-state reaction method, solid-liquid reaction method and so on. However, these methods need tens to hundreds of hours and high cost. Glass crystallization might be another effective way to prepare $Y_{4.67}(SiO_4)_3O$ apatite, but until now there are no reports about the glass ceramics containing $Y_{4.67}(SiO_4)_3O$ apatite.

From the above, many researchers studied the crystallization of the YAS glass system but $Y_{4.67}(SiO_4)_3O$ apatite has not been found and $Y_2Si_2O_7$ is not as single crystalline phase to precipitate in the YAS glass ceramics. In this work, the crystallization behavior of YAS parent glasses with different chemical compositions that were elected according to Y_2O_3-Al_2O_3-SiO_2 phase diagram have been studied in order to prepare YAS glass ceramics precipitated singly/mainly $Y_2Si_2O_7$ or $Y_{4.67}(SiO_4)_3O$ apatite crystal. Besides, the crystallization behavior of stoichiometric parent glass (SPG) having the same stoichiometric ratio with the precipitated crystal and non-stoichiometric parent glass (NSPG) is also investigated and compared in details.

2. Experimental

The glasses were prepared by using the following reagent grade materials, Y_2O_3 (99.9 %), Al_2O_3 (99.9 %), SiO_2 (99.0 %). Table 1 shows the chemical composition of the glasses. According to the Y_2O_3-Al_2O_3-SiO_2 phase diagram (Fig. 1) [12], the chemical compositions of glasses were chosen and named after Y, Y2S, M and YMS. In order to make glass precipitate singly/mainly $Y_2Si_2O_7$ crystal, the Y glass chemical composition was designed to be located in the $Y_2Si_2O_7$ phase region of Y_2O_3-Al_2O_3-SiO_2 phase diagram. The M sample is located in the mullite phase region and the YMS sample is located in the triple eutectic point. The Y sample is elected regarding as standard sample to study the influence of SPG and NSPG on crystallization behavior, because the Y glass ceramic was observed to have only single crystallized phase $Y_2Si_2O_7$ by crystal analysis. Therefore, the SPG (named Y2S) was selected according to a certain molar ratio (Y_2O_3:SiO_2 = 1:2) that was the same with the stoichiometric ratio of $Y_2Si_2O_7$. The ratio is shown in red line in Fig. 1. Besides the certain molar ratio, the Y2S is also determined according to two other requirements. First, the composition can melt into glass by melting at high temperature and cooling at room temperature. Second, the composition should be as close to the Y sample composition as possible so that avoid large crystallization difference caused by component deviation. After multiple experiments, the chemical composition of Y2S sample is identified as $25Y_2O_3$-$25Al_2O_3$-$50SiO_2$ (mol%).

A mixture of the precursor oxide powders (400 g) was mixed in mortar and melted in platinum crucible. The raw materials according to the calculated weight were mixed evenly and ground uniform, then melted at 1550 °C for 3 h. The melt was cast into a preheated graphite mould and then annealed at glass transition temperature for 2 h to eliminate the residual stress in glass structure. The X-ray fluorescence was used to check the resulting glasses chemical composition, and the results agreed with the experimental error of ±3 % with the compositions of the initial batches. The amorphous character of samples was confirmed by X-ray diffraction. The annealed glasses are controlled to crystallize by two-step heat treatment. The glasses were heated firstly at 5 °C/min to nucleation temperature, held for 1 h, and then heated again at 5 °C/min to crystallization temperature and held for 2.5 h, finally cooled down to room temperature by natural cooling. The nucleation and crystallization temperature are determined to be about 20 °C above glass transition temperature (Tg) and crystallization peak temperature (Tc).

Tg and Tc are obtained to draw up the heat treatment schedule by the differential scanning calorimetry (DSC, NETZSCH DSC STA449C). 15 mg of glass powder (particle size of about 80 μm) in an alumina crucible was heated from room temperature to 1400 °C at the heating rate of 10 K/min. In order to study the crystallization of glasses with different chemical compositions, the glasses were cut into strips (5×5×10 mm) then controlled to crystallize by two-step heat treatment. The crystal phases

precipitated were analyzed by X-ray diffractometer (Rigaku XRD Miniflex600) for powdered glass ceramic in 10-80 ° angle range at scanning speed of 4 °/min. In order to excellently study the microstructure, the glass ceramic was polished and its surface was corroded by 4 wt% HF for 30 s at room temperature to observe the microstructure by a scanning electron microscopy (FEI SEM QUANTA400), and prior to characterization all samples were sputtered with gold by using a sputtering machine.

In order to study the relation of glass structure and crystallization behavior, the parent glass was detected by a Fourier transform infrared spectrometer (Shimadzu FT-IR Prestige-21) to measure the infrared absorption spectra in the wavenumber range of 400-4000 cm^{-1} with 2 cm^{-1} resolution, the transmission technique was applied and the samples were prepared as KBr pellets. The IR data were processed by normalization to eliminate the effect of uneven sample thickness during preparing.

3. Results and discussion

3.1. Thermal analysis

Fig. 2 shows the DSC results of four samples including endothermic and exothermic peak at a heating rate of 10 K/min. Glass transition temperature was standardized by calculating the inflection point nearby endothermic peak with the second derivative method. The temperature at the inflection point was defined as the glass transition temperature. The glass transition temperature (Tg) of Y, Y2S, M and YMS samples are 906 °C, 905 °C, 915 °C and 913 °C respectively. Low Tg indicates

more non-bridging oxygens (NBOs) in the glassy structure [18,19]. Through the difference of Tg, it can be known that Y and Y2S glasses have more non-bridging oxygen than M and YMS glasses. The crystallization peak temperature (Tc) of Y, Y2S, M and YMS glass are 1137 °C, 1112 °C, 1191 °C and 1253 °C respectively, it can be also observed that Y2S glass has two crystallization peaks at 1112 °C (Tc) and 1344 °C (Tc2). More interesting, except Y2S glass, there is a small exothermic peak for other glasses (named Tx) between Tg and Tc in DSC curve. This small exothermic peak might be caused by the phase separation of glass during heating process, which will be described in next section. The Tx of Y, M and YMS glasses are 1035 °C, 999 °C and 1015 °C, respectively. The values of Tg, Tx, Tc and Tc2 for all glasses are summarized in table 1, and there is an error of ±1 °C for Tg and Tc.

By comparing glass crystallization peak temperatures (Tc: YMS>M>Y>Y2S) with the temperatures of the liquidus surface (Ts: Y2S>Y>M>YMS) obtained from phase diagram of the Y_2O_3-Al_2O_3-SiO_2 system with plots of the isotherms [20], one can observe an interesting fact that the higher Ts of glass chemical composition locating at phase diagram of the Y_2O_3-Al_2O_3-SiO_2 system, the lower Tc of corresponding glass. With the same chemical composition, the glass obtained at a slower cooling rate would have a lower enthalpy than that obtained using a faster cooling rate [21]. Hence, the faster cooling glass possesses higher enthalpy in glass structure and has better crystallization potential, thereby it can be more easily crystallized and consequently

exhibits lower Tc. In this work, the experiment adopts identical cooling rate, so the chemical composition is the single factor influencing the enthalpy of glass. The glass chemical composition locating at higher Ts may have a higher enthalpy in glass structure and hence its Tc is lower, as a result, corresponding glass obtained at same cooling rate is crystallized more easily.

3.2. Crystallization

Generally, the nucleation temperature for preparing glass ceramics is above 50 °C glass transition temperature. In this work the nucleation temperature of all samples is set as 920 °C for simplicity and then the samples are heat treated at different Tx and Tc. Fig. 3 shows XRD patterns of glasses heat treated according to the heat treatment schedule listed in Table 2. As shown in Fig. 3(a), XRD patterns of Y-1, M-1 and YMS-1 samples heat treated at 920 °C for 2 h and their Tx temperature for 2.5 h are diffuse X-ray peak, showing that they still keep glassy nature and there are no precipitated crystals in glasses after heat treated at nucleation temperature and Tx temperature. Fig. 4 gives the SEM photograph for the heat treated glasses. After heat treatment at 920 °C for 1 h and 1035 °C for 2.5 h, there are some ununiform circular area in Y-1 sample as shown in Fig. 4(a), presumably phase separation is occurred for Y-1 sample combining with no crystal precipitated as shown in Fig. 3(a). Similarly, the phase separation might be occurred in M-1 and YMS-1 samples. Thereby, it can be considered that the exothermic peak for Y, M and YMS glasses between glass transition temperature and crystallization peak

temperature could be attributed to occurrence of phase separation of glass sample during heat process.

After heat treatment at 920 °C for 1 h and 1137 °C (crystallization peak temperature) for 2.5 h, the y-$Y_2Si_2O_7$ crystal is precipitated in Y-2 sample as shown in Fig. 3 (b). Unfortunately, a little diffraction peaks at 25.95 °, 31.12 °, 35.37 ° and 40.91 ° in Y-2 sample appear and are not attributable, but the precipitated crystals in Y-2 sample are mainly the y-$Y_2Si_2O_7$. Comparing the phase separation regions occurred in Y-1 sample (Fig. 4(a)) with the circular regions of crystal precipitated in Y-2 sample (Fig. 4(b)), they are similar in shape. After the same heat treatment time (2.5 h) at different temperature (Tx=1035 °C and Tc=1137 °C), the size of the crystal area in Y-2 sample is somewhat larger than the size of the phase separation area in Y-1sample due to the crystal growth at higher temperature (1137 °C for Y-2 and 1035 °C for Y-1), and the phase separation area is about 7.4 μm (Fig. 4(a), line 1) and 9.6 μm for crystal area (Fig. 4(b), line 2) respectively. Apart from similar shape, the content of Si and Y elements in phase separation area is higher than that near phase separation region (as shown in Fig. 5), the content of Si and Y elements in phase separation area is enriched as formation of phase separation, the content of Si and Y elements are 25.86 and 13.10 (At%) nearby the phase separation region, after occurrence of phase separation they are accumulated to 28.94 and 16.21 (At%) respectively in the phase separation area. Aggregation of Si and Y elements in some small areas serves nucleation and crystal

growth of corresponding crystal such as $Y_2Si_2O_7$ crystal. Therefore, it can be concluded that the crystallization mechanism of Y glass heat treated at 920 °C for 1 h and 1137 °C for 2.5 h is caused by phase separation occurred at lower temperature, and phase separation provides a beneficial condition for crystallization.

As for M and YMS samples, after heat treating at 920 °C for 1 h and their crystallization peak temperature (1191 °C and 1253 °C) for 2.5 h respectively, comparing M-1 with M-2 and YMS-1 with YMS-2 samples, it can be found that M-2 and YMS-2 samples are crystallized at their surface, and they have identical crystal phases including y-$Y_2Si_2O_7$, mullite and cristobalite (Fig. 3 (c)), it is reasonable to conclude that the phase separation occurred also in M and YMS glasses similarly which provides beneficial condition for crystallization of corresponding crystals, while the crystal growth rate for M and YMS is not the same according to their different surface crystalline thickness (Fig. 6 (e) and (f)), the surface crystalline thickness of M-2 glass ceramic is much smaller than YMS-2, suggesting the crystallization rate of YMS glass is much larger than M glass. YMS-3 sample annealed at 920 °C for 1 h and 1253 °C for 0.5 h is also shown in Fig. 6 (g), to compare with YMS-2 glass ceramic obtained at 920 °C for 1 h and 1253 °C for 2.5 h, it is really clear that crystallization of YMS is along sample surface and the crystal growth rate is very fast.

Chemical composition of Y2S sample has the same stoichiometric ratio (Y_2O_3:SiO_2 = 1:2) with the crystal phase $Y_2Si_2O_7$, it has two crystallization peaks at 1112 °C and

1344 °C as listed in Table1, thereby Y2S glass is heat treated at 1112 °C and 1344 °C respectively. Y2S-1 glass ceramic heat treated at 920 °C for 1 h and 1112 °C for 2.5 h is observed to crystallize only $Y_{4.67}(SiO_4)_3O$ crystal (Fig. 3(b)), Y2S-2 glass ceramic heat treated at 920 °C for 1h and 1344 °C for 2.5 h is observed to crystallize y-$Y_2Si_2O_7$ and little $Y_{4.67}(SiO_4)_3O$ crystal (Fig. 3(b)), formation of the little $Y_{4.67}(SiO_4)_3O$ may be occurred around 1112 °C during the sample is heated to 1344 °C. Fig. 4(c) and (d) show the SEM images of the Y2S-1 and Y2S-2 glass ceramics respectively, their microstructures of crystals precipitated in glass ceramics are really different from the crystal microstructure in Y-2 glass ceramic. Obviously, no phase separation exothermic peaks in thermal analysis are found in the Y2S glass (Fig. 2), so the crystallization mechanism of Y2S glass is different from Y glass. Fig. 6 gives the profile photos of the heat treated glasses, it can be found that the Y-2 sample began to crystallize along its surface and then crystals grow inwards the sample (Fig. 6 (a)), and Y2S-1 sample has the same crystallization way with Y-2 sample (Fig. 6 (b)), however, Y2S-2 sample shows overall crystallization process (Fig. 6 (c)) when Y2S glass is heat treated at the second crystallization peak temperature (1344 °C for 2.5 h). To confirm whether the Y2S-2 glass ceramic belongs to surface crystallization or that the rate of crystallization is too fast at second crystallization peak temperature leading to complete crystallization, the Y2S-3 sample is annealed only at 1344 °C for 5 min without at 920 °C for 1 h, as shown in Fig. 6 (d), it is still overall crystallization even though such short heat

treatment duration. Besides, comparing the profile photos of all glass ceramics (Fig.6), it is found that Y2S glass is the most easily crystallized which is well in agreement with DSC results because of the highest enthalpy of Y2S glass. Therefore, it is really interesting for Y2S glass how to control glass ceramics microstructure (surface or overall crystallization) and precipitated crystals (y-$Y_2Si_2O_7$ or $Y_{4.67}(SiO_4)_3O$ crystals).

By the DSC analysis and crystallization behavior for SPG (Y2S) and NSPG (Y, M and YMS) samples, there is an exothermic peak for the NSPG samples caused by phase separation in DSC curve, phase separation of the NSPG samples is occurred when it is heat treated at this temperature (Tx), which lead to the obvious crystallization of NSPG samples as the heat treating temperature is elevated to the crystallization peak temperature (Tc). In the case of SPG sample, there are two exothermic peaks in DSC curve, and no phase separation is observed, while $Y_{4.67}(SiO_4)_3O$ crystal is precipitated along the sample surface when SPG sample is heat treated at the first exothermic peak temperature. Main y-$Y_2Si_2O_7$ and little $Y_{4.67}(SiO_4)_3O$ crystals are precipitated from the SPG sample when SPG sample is annealed at second exothermic peak temperature, and it is the overall crystallization even though very short heat treatment duration (5min) at the second exothermic peak temperature.

3.3. Structure analysis

The FT-IR spectra of the parent glasses in the wavenumber range of 400-1400 cm^{-1}, 400-650 cm^{-1} and 850-1350 cm^{-1} are showed in Fig. 7 (a), (b) and (c), respectively. The

band located in the range of 448-465 cm^{-1} is assigned to bending vibrations of the T-O-T (T=Si or Al) bonds, and another band in the range of 470-510 cm^{-1} is assigned to Si-O-Si bending vibration mode [5,18,22] and overlapped with the former. The overlapped bands at 600-750 cm^{-1} are connected with Si-O-(Si, Al) symmetric stretching vibrations between the tetrahedral. The absorption band centered at 685 cm^{-1} is due to the bending Si-O-Al vibrations as well as to the stretching vibrations of the Al-O bond in the alumino-oxygen tetrahedral, and the shoulder at about 620 cm^{-1} definitely should be associated with the silicon-aluminum-oxygen ring vibrations [23-26]. The absorption band at about 760-800 cm^{-1} represents Si-O-Si symmetric stretching vibration, but a contribution to this absorption band could arise also from tetra-coordinated aluminium [5,27,28]. Besides, the spectral range of 500-600 cm^{-1} is expected to be assigned to Y-O stretching vibration [27]. It can be seen from Fig. 7 (b) that Y and Y2S glasses have lower absorption intensity than the samples of M and YMS at nearby 470 cm^{-1} band belonging to Si-O-Si bending vibration, so Y and Y2S have more non-bridging oxygen and weak network connectivity. Moreover, this band that moved toward higher wavenumber is due to the fact that Y and Y2S have more strong Y-O bonds resulting from high Y/Si ratio.

The intense absorption band in the range of 850-1200 cm^{-1} is the asymmetric stretching vibration of Si-O-Si bonds in the SiO_4 tetrahedron with different numbers of bridging oxygen atoms [15,29,30]. This band comprises the unit Q^n standing for a

silicon tetrahedron containing n bridging oxygen (BO), namely, Q^0 (SiO_4^{4-} monomer), Q^1 ($Si_2O_7^{6-}$ dimmer), Q^2 (SiO_3^{2-} chain), Q^3 ($Si_2O_5^{2-}$ sheet), Q^4 (SiO_2 three-dimensional network) [31]. Besides, this band can be also interpreted as vibration in structural units associated with vibration of aluminosilicate ring formed by Si and Al tetrahedra [23-26]. It can be observed from Fig. 7 (c) that Y and Y2S glasses have higher absorption intensity at nearby 920 cm^{-1} band and lower absorption intensity at nearby 1080 cm^{-1} band than the samples of M and YMS. For more precise quantitative analysis, the absorption band attributed to the Si-O-Si asymmetric stretching vibration is deconvoluted by Guassian model in Origin 8, the bands positions, widths and intensities are independent and unconstraint variables in curve fitting procedure. The R square for all fitting data are more than 99.6 %, and the fitting results of four samples are given in Fig. 8. Table 3 gives the frequencies, areas and area% and these bands at near 900 cm^{-1}, 960 cm^{-1}, 1095 cm^{-1} and 1190 cm^{-1} respectively contributed to Q^1, Q^2, Q^3 and Q^4. Shakeri et al. [18] and Mahdy et al. [5] reported that some little changes such as reduction of bands absorption intensity in CaO-MgO-Al_2O_3-SiO_2 system or Li_2O-Al_2O_3-SiO_2 system by increasing of Y_2O_3 content illustrated the prominent role of Y^{3+} ions as network former in the glass. Noritaka Saito et al. [32] suggested Y^{3+} ions exist as network modifier in the glass according to the results of viscosity of Y-Al-Si-O-N glass melts and Vickers hardness of oxynitride glasses. However, the Y^{3+} ionic radius is larger than Al^{3+} ionic radius [33], so Y^{3+} cations have a priority to occupy

octahedral voids as network modifier. As the Y/Si ratio (shown in Table 1) increases, the bridging oxygen of glasses is decreased, and so Y^{3+} ions serve as network modifier existing in the studied glasses and Y_2O_3 provides free oxygen in yttrium aluminosilicate glass system.

Our group previously calculated the average number of NBO per tetrahedron (NBO/tetrahedron) and average number of bridging corners per tetrahedron (bridges/tetrahedron) by the deconvoluted Raman spectra of high frequency region attributed to the Si-O stretching vibration of [SiO_4] tetrahedron structural units Q^n with 0-4 bridged oxygens for base and rare earth oxides doped soda-lime-silicate glasses [31,34-35]. The expressions are given as follows.

$$X_{NBO/T} = \sum_{i=1}^{3} X_i n_i$$

$$\frac{NBO}{tetrahedron} = \frac{\sum Q^n (4-n)}{[Si+Al]}$$

$$\frac{bridges}{tetrahedron} = \frac{\sum Q^n n}{[Si+Al]}$$

where X_i is the mole fraction of SiO_4 units with n_i non-bridging oxygen per silicon. The deconvoluted infrared spectrum of Si-O-Si asymmetric stretching vibration is analyzed by the above calculation method to study the effect of chemical composition of YAS glass on structure and crystallization behavior. The fraction and content of structure units Q^n, fraction of non-bridging oxygen, average number of NBO per tetrahedron and average number of bridging corners per tetrahedron for the investigated glasses are

summarized in Table 4. It can be observed that as the Y/Si ratio increases in chemical composition of glass, Q^1 and Q^2 are increased, Q^3 and Q^4 are decreased, and the nonbridging oxygen and the bridge per tetrahedron of glasses are increased and decreased respectively, as a result, the whole glass structure connectivity is weakened, which is in agreement with the variation trend of glass transition temperature (as shown in table 1), indicating that increasement of Y/Si ratio in YAS glass makes more nonbridging oxygens in glass and glass structure more open, resulting in glass transition temperature decrease. And according to the report of other scholars [14], $Y_{4.67}(SiO_4)_3O$ unit cell is made up of Y^{3+} and silicon-oxygen tetrahedron and the y-$Y_2Si_2O_7$ unit cell consists of Y^{3+} and $[Si_2O_7]^{6-}$, $[Si_2O_7]^{6-}$ is formed by a bridging oxygen connecting two silicon-oxygen tetrahedron. Thereby, more Q^1 and Q^2 content in glass structure is advantageous to crystallize $Y_{4.67}(SiO_4)_3O$ and y-$Y_2Si_2O_7$ crystal. Consequently, the Y and Y2S glasses is easier to precipitate $Y_{4.67}(SiO_4)_3O$ or y-$Y_2Si_2O_7$ single or main crystal.

4. Conclusion

Crystallization behavior and structure analysis of YAS glasses have been studied in this work. The glass chemical composition locating at the higher temperature of liquidus surface in YAS phase diagram has lower peak crystallization temperature due to the higher enthalpy in glass structure. The crystallization mechanism for NSPG glasses (Y, M and YMS) and the SPG glass (Y2S heat treated at the first exothermic peak

temperature) all belong to surface crystallization, while SPG glass (Y2S heat treated at the second exothermic peak temperature) belong to overall crystallization, and the stoichiometric parent glass having the same stoichiometric ratio with the precipitated crystal, is more easily crystallization than non-stoichiometric parent glass composition. Besides, NSPG glasses (Y, M and YMS) is observed occurrence of phase separation when it is annealed at the exothermic peak temperature between glass transition temperature and crystallization peak temperature, and their crystallization behavior at crystallization peak temperature is caused by the phase separation. Y-2 and Y2S-2 glass ceramics are observed mainly existing y-$Y_2Si_2O_7$ crystal, Y2S-1 glass ceramic is precipitated only $Y_{4.67}(SiO_4)_3O$ apatite. Y and Y2S glasses are easier to precipitate $Y_{4.67}(SiO_4)_3O$ or y-$Y_2Si_2O_7$ single or mainly crystal, which mainly because more Q^1 and Q^2 content in glass structure is advantageous to crystallize $Y_{4.67}(SiO_4)_3O$ and y-$Y_2Si_2O_7$ crystal in view of crystal structure point. Consequently, this work has a technical guiding role in controlling the crystallization process (overall and surface crystallization) and the types of precipitated crystals of YAS glass for different application potentials.

Acknowledgements

This project is financially supported by National Natural Science Foundation of China (51974168, 51662033 and 51362019), Natural Science Foundation of the Inner Mongolia Autonomous Region (2016JQ05).

Author Information

*Corresponding author:

Pro. Mitang Wang: E-mail: btwmt@126.com, Tel: +86-15848255894

References

[1] S. Tanabe, K. Hirao, N. Soga, Elastic properties and molar volume of rare-earth aluminosilicate glasses, J. Am. Ceram. Soc. 75 (2010) 503-506, doi:10.1111/j.1151-2916.1992.tb07833.x.

[2] S. Hampshire, M. J. Pomeroy, Grain boundary glasses in silicon nitride: a review of chemistry, properties and crystallisation, J. Eur. Ceram. Soc. 32 (2012) 1925-1932, doi:https://doi.org/10.1016/j.jeurceramsoc.2011.12.023.

[3] M. Herrmann, W. Lippmann, A. Hurtado, Y_2O_3-Al_2O_3-SiO_2-based glass-ceramic fillers for the laser-supported joining of SiC, J. Eur. Ceram. Soc. 34 (2014) 1935-1948, doi:https://doi.org/10.1016/j.jeurceramsoc.2014.01.019.

[4] Y. J. Lin, S. H. Tu, Joining of mullite ceramics with yttrium aluminosilicate glass interlayers, Ceram. Int. 35 (2009) 1311-1315.

[5] E. A. Mahdy, S. Ibrahim, Influence of Y_2O_3 on the structure and properties of calcium magnesium aluminosilicate glasses, J. Mol. Struct. 1027 (2012) 81-86, doi:https://doi.org/10.1016/j.molstruc.2012.05.055.

[6] E. M. Erbe, D. E. Day, Chemical durability of Y_2O_3-Al_2O_3-SiO_2 glasses for the in vivo delivery of beta radiation, J. Biomed. Mater. Res. A 27 (1993) 1301, doi:10.1002/jbm.820271010.

[7] M. Kawashita, R. Shineha, H. M. Kim, T. Kokubo, Y. Inoue, N. Araki, Y. Nagata, M.

Hiraoka, Y. Sawada, Preparation of ceramic microspheres for in situ radiotherapy of deep-seated cancer, Biomaterials 24 (2003) 2955-2963, doi: 10.1016/S0142-9612(03)00094-2.

[8] A. Domanická, R. Klement, A. Prnová, K. Bodišová, D. Galusek, Luminescent rare-earth ions doped Al_2O_3-Y_2O_3-SiO_2 glass microspheres prepared by flame synthesis, Ceram. Int. 40 (2014) 6005-6012, doi:https://doi.org/10.1016/j.ceramint.2013.11.049.

[9] N. Sadiki, J. P. Coutures, C. Fillet, J. L. Dussossoy, Crystallization of lanthanum and yttrium aluminosilicate glasses, J. Nucl. Mater. 348 (2006) 70-78, doi:https://doi.org/10.1016/j.jnucmat.2005.09.003.

[10] A. V. Kir'Yanov, A. Halder, Y. O. Barmenkov, S. Das, A. Dhar, S. K. Bhadra, V. V. Koltashev, V. G. Plotnichenko, M. C. Paul, Distribution of bismuth and bismuth-related centers in core area of Y-Al-SiO_2: Bi fibers, J. Lightwave Technol. 33 (2015) 3649-3659, doi:10.1109/JLT.2015.2449084.

[11] A. V. Kir'Yanov, D. Dutta, Y. O. Barmenkov, S. Das, A. Dhar, V. V. Koltashev, V. G. Plotnichenko, M. C. Paul, Basic and peculiar properties of chromium-magnesium Co-doped YAS-based optical fibers, IEEE J. Quantum Elect. 52 (2016) 1-12, doi:10.1109/JQE.2016.2568750.

[12] O. Fabrichnaya, H. J. Seifert, R. Weiland, T. Ludwig, F. Aldinger, A. Navrotsky, Phase equilibria and thermodynamics in the Y_2O_3-Al_2O_3-SiO_2 system, Z. Metallkd, 92 (2001) 1083-1097.

[13] S. Ahmad, T. Ludwig, M. Herrmann, M. M. Mahmoud, W. Lippmann, H. J. Seifert, Phase evaluation during high temperature long heat treatments in the Y_2O_3-Al_2O_3-SiO_2 system, J. Eur. Ceram. Soc. 34 (2014) 3835-3840, doi:https://doi.org/10.1016/j.jeurceramsoc.2014.05.025.

[14] Z. Q. Sun, M. S. Li, Y, C. Zhou, Recent progress on synthesis, multi-scale structure, and properties of Y-Si-O oxides, Int. Mater. Rev. 59 (2014) 357-383, doi:10.1002/chin.201513295.

[15] W. Zhu, H. Jiang, H. Zhang, Y. Liu, Effect of TiO_2 and CaF_2 on the crystallization behavior of Y_2O_3-Al_2O_3-SiO_2 glass ceramics, Ceram. Int. 44 (2018) 6653-6658, doi:10.1016/j.ceramint.2018.01.076.

[16] H. Okudera, Y. Masubuchi, S. Kikkawa, A. Yoshiasa, Structure of oxide ion-conducting lanthanum oxyapatite, $La_{9.33}(SiO_4)_6O_2$, Solid State Ionics 176 (2005) 1473-1478, doi:https://doi.org/10.1016/j.ssi.2005.02.014.

[17] T. Liao, T. Sasaki, S. Suehara, Z. Sun, Position preference and diffusion path of an oxygen ion in apatite-type lanthanum silicate $La_{9.33}Si_6O_{26}$: a density functional study, J. Mater. Chem. 21 (2011) 3234-3242, doi:10.1039/C0JM02473B.

[18] M. S. Shakeri, M. Rezvani, Optical band gap and spectroscopic study of lithium alumino silicate glass containing Y^{3+} ions, Spectrochim. Acta A 79 (2011) 1920-1925, doi:https://doi.org/10.1016/j.saa.2011.05.090.

[19] K. Singh, N. Gupta, O. P. Pandey, Effect of Y2O3 on the crystallization behavior of SiO_2-MgO-B_2O_3-Al_2O_3 glasses, J. Mater. Sci. 42 (2007) 6426-6432, doi:10.1007/s10853-006-1188-z.

[20] I. A. Bondar, F. Ya. Galakhov, Phase equilibria in the system Y_2O_3-Al_2O_3-SiO_2, Russ Chem B+ 13 (1964) 1231-1232, doi:10.1007/BF00863139.

[21] Shelby J E. Introduction to Glass Science and Technology, Second ed., Royal Society of Chemistry, Cambridge, 2005.

[22] Z. Yang, Q. Lin, S. Lu, Y. He, G. Liao, Y. Ke, Effect of CaO/SiO_2 ratio on the preparation and crystallization of glass-ceramics from copper slag, Ceram. Int.

40(2014)7297-7305, doi: 10.1016/j.ceramint.2013.12.071.

[23] M. Sitarz, W. Mozgawa, M. Handke, Rings in the structure of silicate glasses, J. Mol. Struct. 511-512 (1999) 281-285. doi: 10.1016/S0022-2860(99)00169-6.

[24] M. Sitarz, The structure of simple silicate glasses in the light of middle infrared spectroscopy studies, J. Non-Cryst. Solids 357 (2011) 1603-1608. doi: 10.1016/j.jnoncrysol.2011.01.007.

[25] M. Sitarz, M. Handke, W. Mozgawa, Identification of silicooxygen rings in SiO_2 based on IR spectra, Spectrochim Acta A 56 (2000) 1819-1823. doi: 10.1016/S1386-1425(00)00241-9.

[26] M. Sitarz, M. Handke, W. Mozgawa, E. Galuskin, I. Galuskina, The non-ring cations influence on silicooxygen ring vibrations, J. Mol. Struct. 555 (2000) 357-362. doi: 10.1016/S0022-2860(00)00621-9.

[27] D. Eniu, S. Simon, Structural properties of melt versus sol-gel derived yttrium aluminosilicate systems, Ceram. Int. 44 (2018) 9581-9584, doi:10.1016/j.ceramint.2018.02.181.

[28] Y. Li, K. Liang, J. Cao, B. Xu, Spectroscopy and structural state of V^{4+} ions in lithium aluminosilicate glass and glass-ceramics, J. Non-Cryst. Solids 356 (2010) 502-508, doi:10.1016/j.jnoncrysol.2009.12.018.

[29] J. Zhao, Y. Lu, J. Kang, Y. Qu, G. A. Khater, S. Li, Y. Wang, Y. Yue, Effect of Y_2O_3 and La_2O_3 on structure and dielectric properties of aluminoborosilicate glasses, J. Non-Cryst. Solids 496 (2018) 1-5, doi:10.1016/j.jnoncrysol.2018.05.020.

[30] F. Pei, H. Guo, P. Li, B. Yan, J. Li, P. Yang, G. Zhu, Influence of low magnesia content on the CaO-Al_2O_3-SiO_2 glass-ceramics: Its crystallization behaviour, microstructure and physical properties, Ceram. Int. 44(2018)20132-20139, doi:

10.1016/j.ceramint.2018.07.306.

[31] M. Wang, J. Cheng, M. Li, F. He, Raman spectra of soda-lime-silicate glass doped with rare earth, Physica B 406 (2011) 3865-3869, doi:10.1016/j.physb.2011.07.014.

[32] N. Saito, K. Kai, S. Furusho, K. Nakashima, K. Mori, Properties of nitrogen-containing yttria-alumina-silica melts and glasses, J. Am. Ceram. Soc. 67 (2003) 40-46, doi:10.2320/jinstmet1952.67.1_40.

[33] K. Singh, N. Gupta, O. P. Pandey, Effect of Y_2O_3 on the crystallization behavior of SiO_2-MgO-B_2O_3-Al_2O_3 glasses, J. Mater. Sci. 42 (2007) 6426-6432, doi:10.1007/s10853-006-1188-z.

[34] M. Wang, M. Li, J. Cheng, F. He, Z. Liu, Y. Hu, Free volume and structure of Gd_2O_3 and Y_2O_3 co-doped silicate glasses, J. Non-Cryst. Solids 379 (2013)145-149, doi: 10.1016/j.jnoncrysol.2013.08.003.

[35] M. Wang, M. Li, J. Cheng, F. He, Structure and viscosity of soda lime silicate glasses with varying Gd_2O_3 content, J. Mol. Struct. 1063 (2014) 139-144, doi: 10.1016/j.molstruc.2014.01.062.

Figure captions

Fig. 1 The Y_2O_3-Al_2O_3-SiO_2 phase diagram. YAM: Y_4Al_2O9; YAP: $YAlO_3$; YAG: $Y_3Al_5O_{12}$; Mull: Mullite; TR: Tridymite; Y, Y2S, M and YMS are the studied glasses in this work.

Fig. 2 DSC curves of glasses Y, Y2S, M and YMS. Tc is the first crystallization peak temperature; Tc2 the second crystallization peak temperature; Tx is the temperature between glass transition temperature (Tg) and the first crystallization peak temperature.

Fig. 3 XRD patterns of the heat treated glasses

Fig. 4 SEM micrographs (a) Y-1, (b) Y-2, (c) Y2S-1, (d) Y2S-2

Fig. 5 EDS results of Si and Y elements in and nearby the phase separation area for Y-1 sample

Fig. 6 Profile photos of the annealed glasses (a)Y-2, (b) Y2S-1, (c)Y2S-2, (d)Y2S-3, (e) M-2, (f) YMS-2, (g) YMS-3

Fig. 7 IR spectra of the studied parent glass (a) 400-1400 cm^{-1}, (b) 400-650 cm^{-1}, (c) 850-1350 cm^{-1}

Fig. 8 Deconvoluted IR spectrum at 850-1300 cm^{-1} of YAS glasses: (a) Y, (b) Y2S, (c) M, (d) YMS

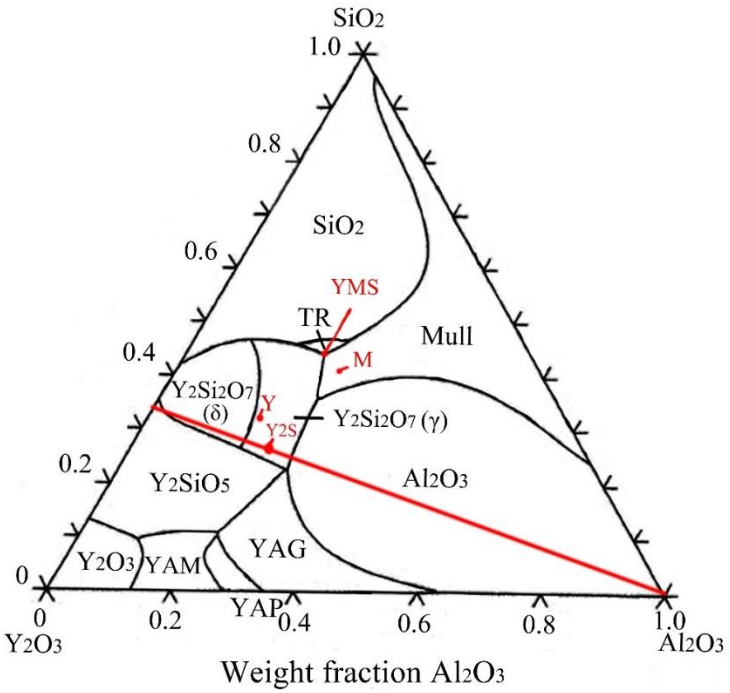
SiO2
1.0
0.8
0.6
0.4
0.2
0
SiO2
YMS
TR
M
Mull
Y2Si2O7 (δ)
Y
Y2S
Y2Si2O7 (γ)
Y2SiO5
Al2O3
Y2O3
YAM
YAG
YAP
0
0.2
0.4
0.6
0.8
1.0
Y2O3
Al2O3
Weight fraction Al2O3

Fig. 1

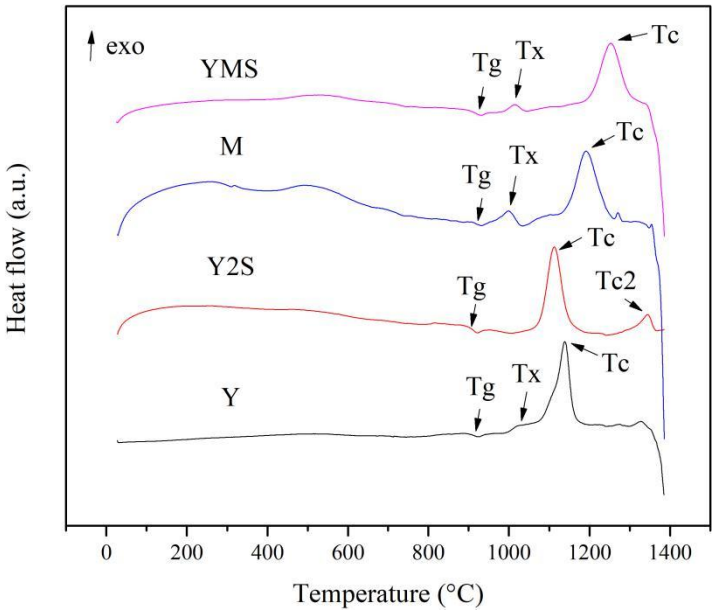
exo
YMS
M
Y2S
Y
Tg
Tx
Tc
Tc2
Heat flow (a.u.)
0
200
400
600
800
1000
1200
1400
Temperature (°C)

Fig. 2

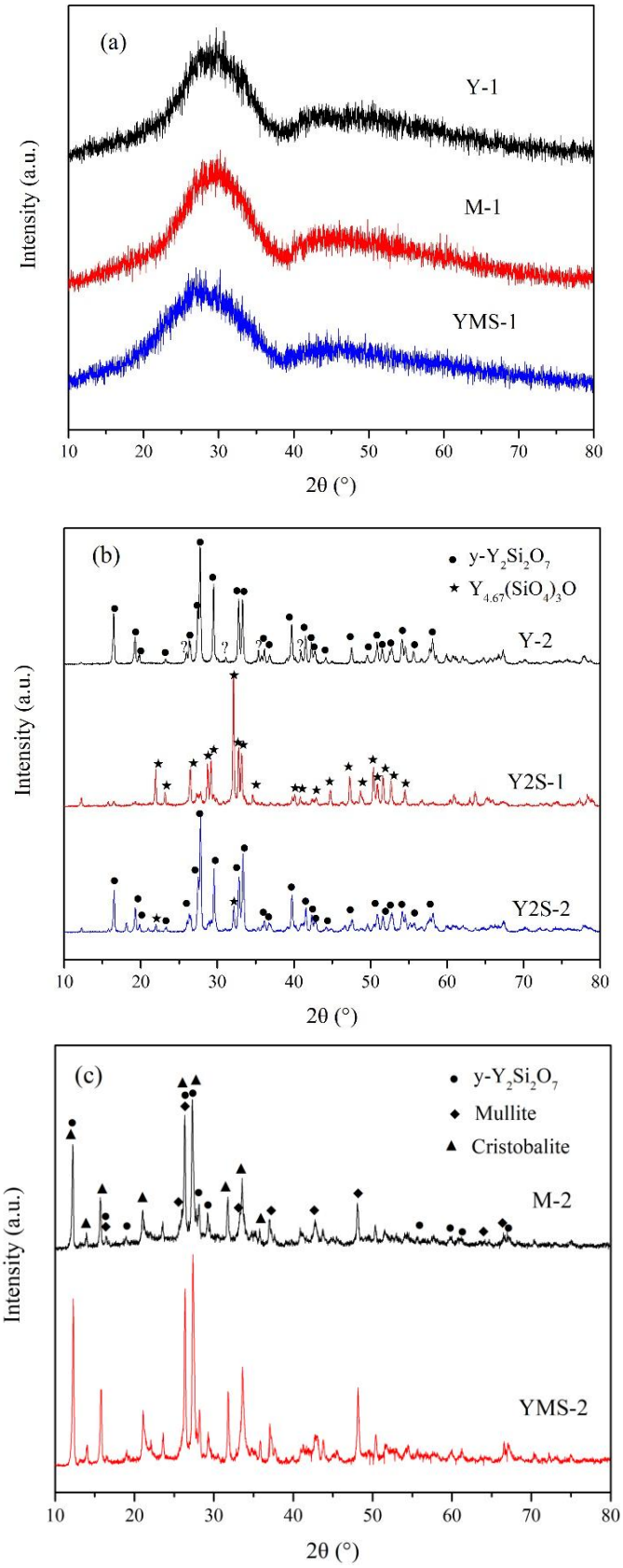
(a)
Y-1
M-1
YMS-1
Intensity (a.u.)
10
20
30
40
50
60
70
80
2θ (°)
(b)
• y-$Y_2Si_2O_7$
★ $Y_{4.67}(SiO_4)_3O$
Y-2
Y2S-1
Y2S-2
Intensity (a.u.)
2θ (°)
(c)
• y-$Y_2Si_2O_7$
◆ Mullite
▲ Cristobalite
M-2
YMS-2
Intensity (a.u.)
2θ (°)

Fig. 3

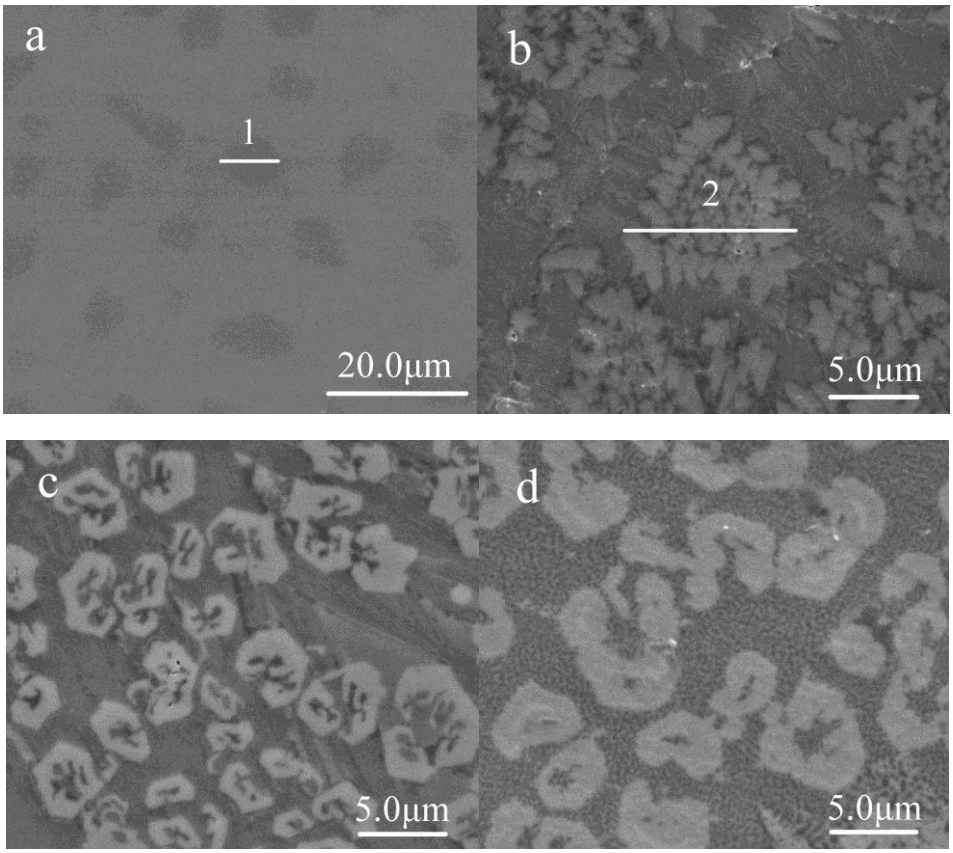
a
1
20.0μm
b
2
5.0μm
c
5.0μm
d
5.0μm

Fig. 4

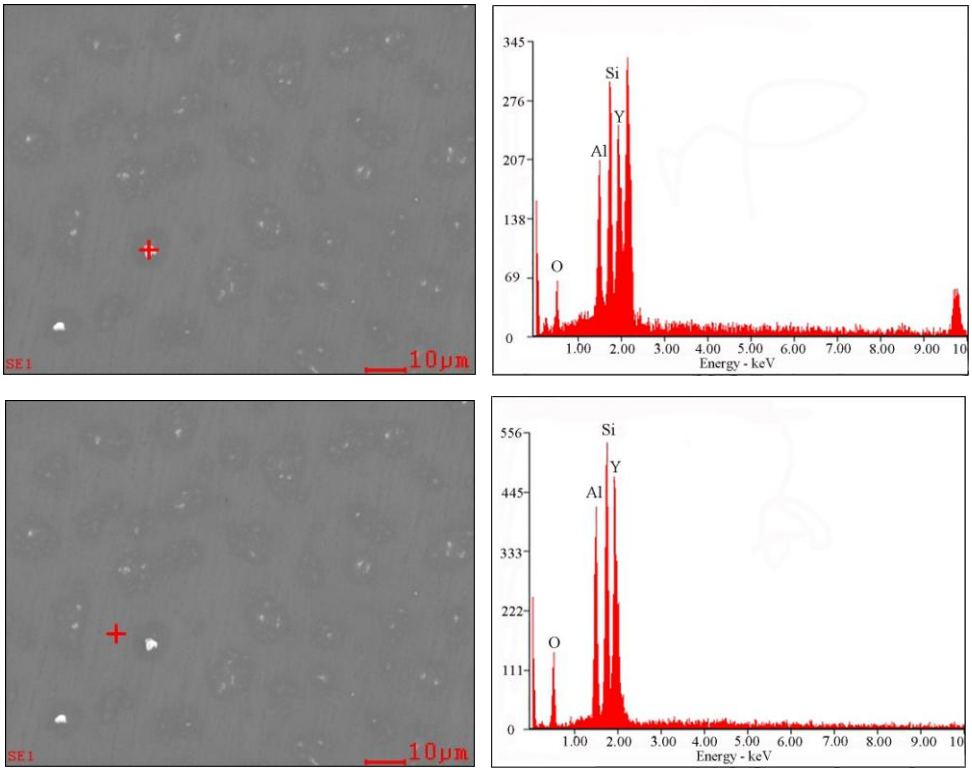
SE1
10μm
345
276
207
138
69
0
Si
Y
Al
O
1.00 2.00 3.00 4.00 5.00 6.00 7.00 8.00 9.00 10
Energy - keV
SE1
10μm
556
445
333
222
111
0
Si
Y
Al
O
1.00 2.00 3.00 4.00 5.00 6.00 7.00 8.00 9.00 10
Energy - keV

Fig. 5

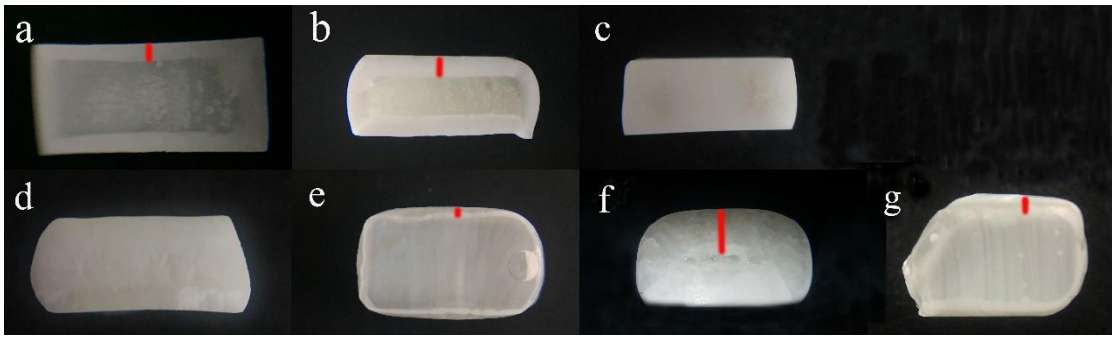
a
b
c
d
e
f
g

Fig. 6

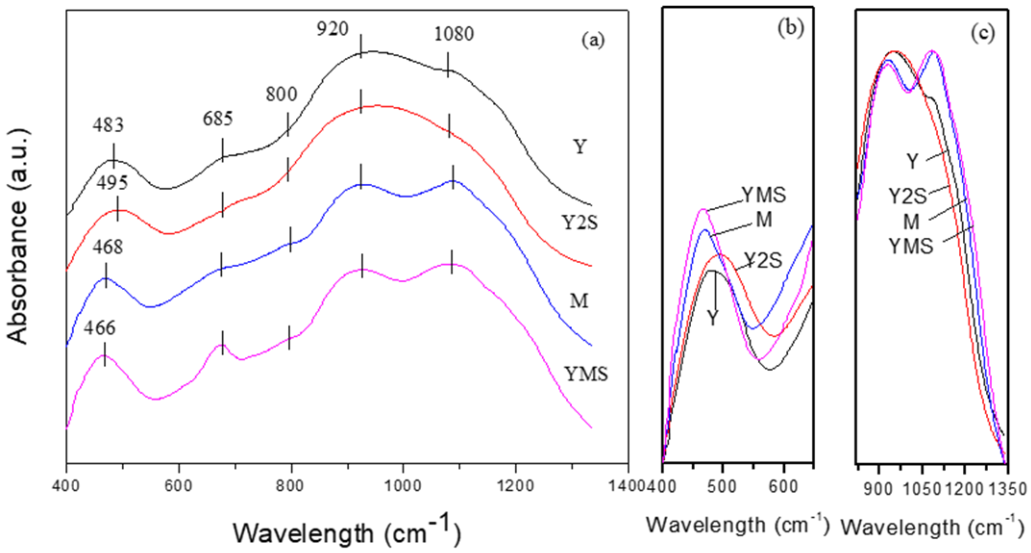
(a)
(b)
(c)
920
1080
800
685
483
495
468
466
Y
Y2S
M
YMS
Absorbance (a.u.)
400
600
800
1000
1200
1400
Wavelength (cm-1)
500
900
1050
1350

Fig. 7

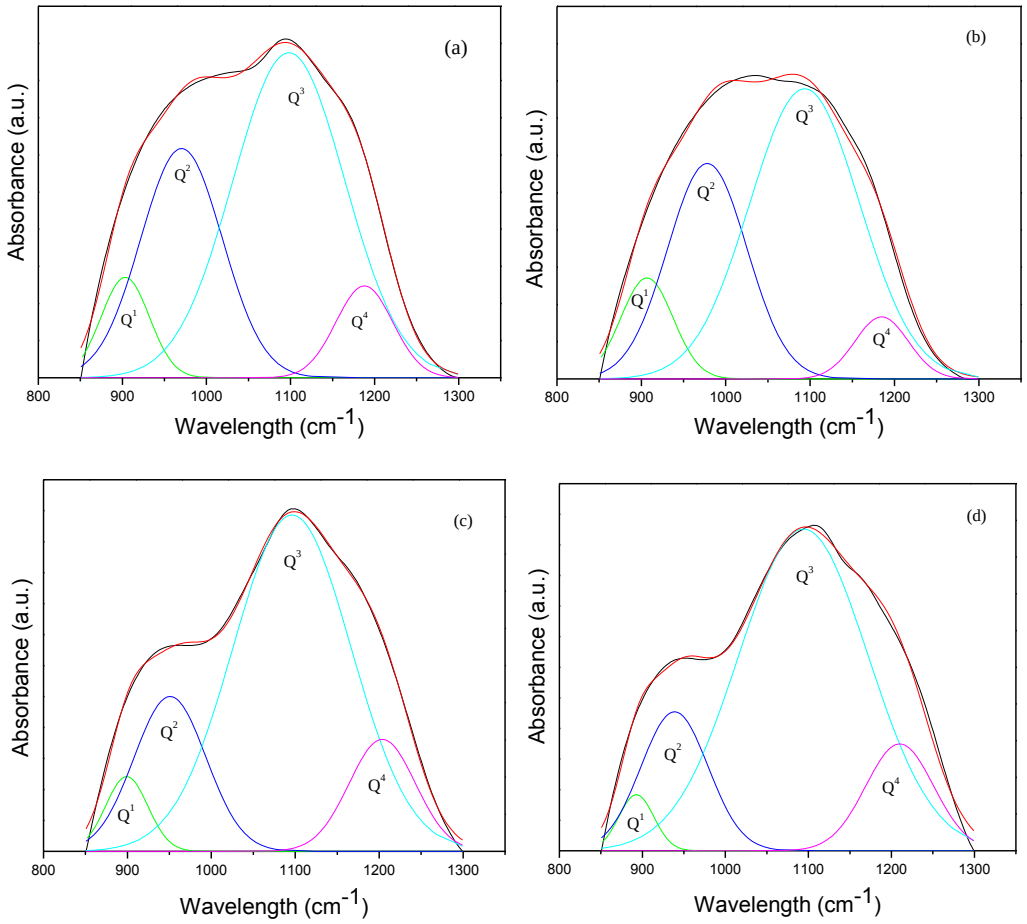
(a)
(b)
(c)
(d)
Absorbance (a.u.)
Wavelength (cm-1)
Q1
Q2
Q3
Q4
800
900
1000
1100
1200
1300

Fig. 8

Table 1. Chemical compositions (mol %), glass transition and crystallization temperatures of glass samples

Sample	Y_2O_3	Al_2O_3	SiO_2	Y/Si	Tg(°C)	Tx(°C)	Tc(°C)	Tc2(°C)
Y	22	19	59	0.74	906	1035	1137	—
Y2S	25	25	50	1.00	905	—	1112	1344
M	11.89	23.17	64.94	0.37	915	999	1191	—
YMS	12.62	19.21	68.17	0.37	913	1015	1253	—

Table 2. Heat treatment schedules and crystallization behavior for glasses

Sample	Annealing(T, t)		Observed phase
Y-1	920 °C, 1 h	1035 °C, 2.5 h	No crystallization
Y-2	920 °C, 1 h	1137 °C, 2.5 h	y-$Y_2Si_2O_7$
Y2S-1	920 °C, 1 h	1112 °C, 2.5 h	$Y_{4.67}(SiO_4)_3O$
Y2S-2	920 °C, 1 h	1344 °C, 2.5 h	y-$Y_2Si_2O_7$+(little) $Y_{4.67}(SiO_4)_3O$
Y2S-3	920 °C, 0 h	1344 °C, 5 min	y-$Y_2Si_2O_7$+(little) $Y_{4.67}(SiO_4)_3O$
M-1	920 °C, 1 h	999 °C, 2.5 h	No crystallization
M-2	920 °C, 1 h	1191 °C, 2.5 h	y-$Y_2Si_2O_7$ + mullite + cristobalite
YMS-1	920 °C, 1 h	1015 °C, 2.5 h	No crystallization
YMS-2	920 °C, 1 h	1253 °C, 2.5 h	y-$Y_2Si_2O_7$ + mullite + cristobalite
YMS-3	920 °C, 1 h	1253 °C, 0.5 h	y-$Y_2Si_2O_7$ + mullite + cristobalite

y-$Y_2Si_2O_7$ (JCPDS-22-1103); $Y_{4.67}(SiO_4)_3O$ (JCPDS-30-1457); mullite (JCPDS-02-0431); cristobalite (JCPDS-03-0276).

Table 3 Frequencies (V/cm^{-1}), areas (A) and area % (A%) of IR bands obtained from the deconvolution fitting

	Y	Y2S	M	YMS
V1	903	907	899	893
V2	970	978	951	939
V3	1098	1094	1096	1094
V4	1188	1185	1204	1210
A1	9.41	10.14	7.42	4.74
A2	37.32	33.96	26.62	22.65
A3	72.98	63.37	95.50	102.25
A4	10.48	6.61	17.78	17.65
A1%	7.22	8.88	5.04	3.21
A2%	28.66	29.77	18.07	15.38
A3%	56.06	55.55	64.82	69.42
A4%	8.05	5.79	12.07	11.98

Table 4 Fraction (X^n%) and content (Q^n/%) of structure units, average number of NBO per tetrahedron and average number of bridging corners per tetrahedron

	Y	Y2S	M	YMS
X^1%	8.30	10.21	5.80	3.69
X^2%	29.23	30.37	18.43	15.69
X^3%	58.30	57.77	67.41	72.20
X^4%	4.16	1.65	8.36	8.42
Q^1	8.05	10.21	6.45	3.94
Q^2	28.36	30.37	20.51	16.72
Q^3	56.55	57.77	75.02	76.95
Q^4	2.46	0.83	5.43	5.74
NBO/tetrahedron	1.42	1.49	1.22	1.15
bridges/tetrahedron	2.58	2.51	2.78	2.85

Figure captions

Fig. 1 The Y_2O_3-Al_2O_3-SiO_2 phase diagram. YAM: Y_4Al_2O9; YAP: $YAlO_3$; YAG: $Y_3Al_5O_{12}$; Mull: Mullite; TR: Tridymite; Y, Y2S, M and YMS are the studied glasses in this work.

Fig. 2 DSC curves of glasses Y, Y2S, M and YMS. Tc is the first crystallization peak temperature; Tc2 the second crystallization peak temperature; Tx is the temperature between glass transition temperature (Tg) and the first crystallization peak temperature.

Fig. 3 XRD patterns of the heat treated glasses

Fig. 4 SEM micrographs (a) Y-1, (b) Y-2, (c) Y2S-1, (d) Y2S-2

Fig. 5 EDS results of Si and Y elements in and nearby the phase separation area for Y-1 sample

Fig. 6 Profile photos of the annealed glasses (a)Y-2, (b) Y2S-1, (c)Y2S-2, (d)Y2S-3, (e) M-2, (f) YMS-2, (g) YMS-3

Fig. 7 IR spectra of the studied parent glass (a) 400-1400 cm^{-1}, (b) 400-650 cm^{-1}, (c) 850-1350 cm^{-1}

Fig. 8 Deconvoluted IR spectrum at 850-1300 cm^{-1} of YAS glasses: (a) Y, (b) Y2S, (c) M, (d) YMS